# Red luminescence and ferromagnetism in europium oxynitridosilicates with β-$K_2SO_4$ structure

Ashley P. Black, Kristin A. Denault, Judith Oró-Solé, Alejandro R. Goñi, and Amparo Fuertes

## Supplementary Information

### Experimental

Polycrystalline samples of $LaM_{1-x}Eu_xSiO_3N$ (x=0, 0.01, 0.02, 0.05, 0.1) and $La_{1-x}Ce_xMSiO_3N$ (x=0, 0.01, 0.02, 0.05, 0.1) (M= Sr) were prepared by solid state reaction in $N_2/H_2$ (95%:5%, Air liquide, 99.999%) of stoichiometric mixtures of $La_2O_3$ (Aldrich, 99.99 %), SrO or BaO, $Si_3N_4$ (α-phase, Alfa Aesar, 99.9%), $SiO_2$ (Aldrich, 99.995 %) and $Eu_2O_3$ (Aldrich, 99.99 %) or $CeO_2$ (Aldrich, 99.995 %). $LaEuSiO_3N$ was prepared from stoichiometric mixtures of $La_2O_3$, $Si_3N_4$ and $Eu_2O_3$ adding 1.4 % (w/w) of graphitic C (Aldrich) as oxygen scavenger. $La_2O_3$, $Eu_2O_3$, $SiO_2$ and $CeO_2$ were previously dried at 950 °C for 4 h for dehydration. SrO and BaO were prepared by overnight decomposition of $SrCO_3$ (Alfa Aesar, 99.994%) and $BaCO_3$ (Aldrich 99.99 %) at 1000 °C under a dynamic vacuum of $5x10^{-2}$ mbar. Handling of SrO and BaO was carried out in a Glovebox under recirculating argon atmosphere. The powders were thoroughly mixed in an agate mortar for 30 min, pressed into a pellet, placed in a molybdenum crucible and covered with a zirconium foil as oxygen/water scavenger. The mixtures were fired at 1350 °C (for M=Sr, Eu) or 1500 °C (for M=Ba) during 3 to 9 h with heating and cooling rates of 300°C/h. N contents were determined by combustion analysis using a Thermo Fisher Scientific instrument and by thermogravimetric analysis in pure oxygen using a NETZSCH -STA 449 F1 Jupiter equipment.

Powder X-ray diffraction data were collected on a Rigaku diffractometer using Cu Kα radiation (λ= 1.5418 Å). Powder neutron diffraction data from a 0.5 g $LaBaSiO_3N$ sample were recorded at room temperature on the high-resolution diffractometer HRPD at the ISIS spallation source, Rutherford Appleton Laboratory, U.K. Rietveld refinements were performed using the program Fullprof. Structural models from neutron diffraction data were refined simultaneously against data collected from backscattering and 90° detector banks, which provide *d*-spacing ranges of 0.6 – 2.6 Å and 0.9 – 3.8 Å, respectively. Electron diffraction micrographs were obtained in a JEOL 1210 transmission electron microscope operating at 120 KV, equipped with a side-entry 60/30° double tilt GATHAN 646 specimen holder. The samples were prepared by dispersing the powders in hexane and depositing of a droplet of this suspension on a carbon coated holey film supported on a copper grid.

Diffuse reflectance spectra were registered at room temperature on a UV-Vis-NIR Varian Cary 5000 spectrophotometer, with operational range of 190-3300 nm. The excitation spectra were measured on a Horiba Jobin Yvon FluoroMax-4 spectrofluorometer equipped with an integrating sphere, a xenon source, a photomultiplier detector (range 200 nm to 850 nm) and a photodiode reference detector. The wavelength range is 200 nm to 950 nm. Photoluminescence (PL) spectra were measured at room temperature using the 405 nm line of a solid-state laser for excitation and collected using a LabRam HR800 spectrometer equipped with a charge-coupled device detector. PL spectra were corrected for the spectral response of the spectrometer by normalizing each spectrum employing the detector and grating characteristics. The incident light power density was about 1 $W/cm^2$.

Magnetic measurements were performed between 2 and 300 K in fields of 0.0025 and 0.5 T using a Quantum Design SQUID magnetometer. M(H) curves were measured up to 7 T for temperatures between 2 K and 50 K.

**Table S1. Crystallographic and refinement data for $LaSrSiO_3N$ and $LaBaSiO_3N$**

| | $LaSrSiO_3N$ | $LaEuSiO_3N$ | $LaBaSiO_3N$ |
|---|---|---|---|
| Radiation | X-Ray Cu $k_\alpha$ | X-Ray Cu $k_\alpha$ | Neutron |
| T(K) | 298 | 298 | 298 |
| Space group | Pmnb | Pmnb | Pmnb |
| a(Å) | 5.64362(14) | 5.63246(14) | 5.733(4) |
| b(Å) | 7.10719(17) | 7.11675(18) | 7.316(5) |
| c(Å) | 9.8062(2) | 9.7998(2) | 9.902(7) |
| V(Å$^3$) | 393.329(16) | 392.825(17) | 415.3(5) |
| $N_p$, $N_{ireff}$[(a)] | 4751, 264 | 4751, 240 | 1911, 281 |
| $P_p$, $P_i$, $P_g$[(b)] | 9, 17, 8 | 9, 15, 8 | 14, 18, 11 |
| $R_{Bragg}$, $R_f$, $\chi^2$ | 5.37, 4.52, 1.67 | 6.24, 4.62, 1.70 | 5.30, 4.4, 1.71 |
| $R_p$, $R_{wp}$, $R_{ex}$[(c)] | 9.65, 13.2, 14.9 | 9.19, 12.2, 9.36 | 2.43, 2.69, 2.06 |

(a) $N_p$, $N_{ireff}$ refer to the number of experimental points and independent reflections.

(b) $P_p$, $P_i$, $P_g$, refer to the number of profile, intensity-affecting and global refined parameters, respectively.

(c) Conventional Rietveld R-factors ($R_p$, $R_{wp}$ , $R_{exp}$) in %.

**Table S2. Atomic coordinates, cation and anion occupancies for $LaSrSiO_3N$[(a)]**

| **Site** | **Wyckoff position** | **x** | **y** | **z** | **occupation factor** |
|---|---|---|---|---|---|
| La1/ Sr1 | 4c | 0.25 | 0.6552(3) | 0.5782(3) | 0.242(3)/0.758 |
| La2/ Sr2 | 4c | 0.25 | 0.0078(3) | 0.30391(19) | 0.758/ 0.242 |
| Si | 4c | 0.25 | 0.2192(11) | 0.5828(12) | 1 |
| O1/N1 | 4c | 0.25 | 0.992(2) | 0.5663(17) | 1/0 |
| O2/N2 | 4c | 0.25 | 0.316(3) | 0.436(2) | 0.5/0.5 |
| O3/N3 | 8d | 0.014(2) | 0.2874(17) | 0.6652(19) | 0.75/0.25 |

(a) Estimated standard deviations in parentheses are shown once for each independent variable. La/Sr occupation factors were refined subject to the ideal stoichiometry. O/N occupation factors were considered fixed to those obtained in $LaBaSiO_3N$ from neutron diffraction. Refined isotropic B-factors were 1.01(7) Å$^2$ for La/Sr atoms, 1.32(18) Å$^2$ for silicon and 2.1(2) Å$^2$ for anions.

**Table S3. Atomic coordinates, cation and anion occupancies for $LaEuSiO_3N$[(a)]**

| **Site** | **Wyckoff position** | **x** | **y** | **z** | **occupation factor** |
|---|---|---|---|---|---|
| La1/ Eu1 | 4c | 0.25 | 0.6547(3) | 0.5780(2) | 0.188(18)/0.812 |
| La2/ Eu2 | 4c | 0.25 | 0.0067(3) | 0.30338(19) | 0.812/ 0.188 |
| Si | 4c | 0.25 | 0.2203(13) | 0.5826(14) | 1 |
| O1/N1 | 4c | 0.25 | 0.994(3) | 0.569(2) | 1/0 |
| O2/N2 | 4c | 0.25 | 0.312(4) | 0.430(3) | 0.5/0.5 |
| O3/N3 | 8d | 0.015(3) | 0.283(2) | 0.659(2) | 0.75/0.25 |

(a) Estimated standard deviations in parentheses are shown once for each independent variable. La/Eu occupation factors were refined subject to the ideal stoichiometry. O/N occupation factors were fixed to those obtained in $LaBaSiO_3N$ from neutron diffraction. Refined isotropic B-factors were 1.03(7) Å$^2$ for La/Eu atoms, 1.06(7) Å$^2$ for silicon and 2.6(3) Å$^2$ for anions.

**Table S4. Bond distances and cell parameters for $LaSrSiO_3N$, $LaEuSiO_3N$, $LaBaSiO_3N$ (this work) and related silicates with β-$K_2SO_4$ structure.**[(a)]

| | $LaSrSiO_3N$ | $Sr_2SiO_4$ | $LaEuSiO_3N$ | $Eu_2SiO_4$ | $LaBaSiO_3N$ | $Ba_2SiO_4$ |
|---|---|---|---|---|---|---|
| M1-X1 | 2.397(14) | 2.380(9) | 2.42(2) | 2.416(19) | 2.500(9) | 2.640(7) |
| M1-X2 | 2.79(2) | 2.775(7) | 2.84(3) | 2.83(2) | 2.920(12) | 3.083(7) |
| M1-X2 (x2) | 2.8326(18) | 2.846(6) | 2.827(3) | 2.838(1) | 2.870(2) | 2.915(7) |
| M1-X3 (x2) | 3.055(13) | 3.019(7) | 3.063(15) | 3.013(11) | 3.166(8) | 3.174(7) |
| M1-X3 (x2) | 2.998(17) | 2.985(7) | 3.038(19) | 2.997(12) | 3.036(12) | 3.060(7) |
| M1-X3 (x2) | 2.843(17) | 2.849(6) | 2.796(19) | 2.821(12) | 2.857(12) | 2.904(7) |
| Average | 2.868 | 2.855 | 2.869(16) | 2.858 | 2.928 | 2.983 |
| M2-X1 | 2.575(17) | 2.602(9) | 2.61(2) | 2.607(17) | 2.589(10) | 2.846(7) |
| M2-X1 (x2) | 3.096(7) | 3.111(3) | 3.081(8) | 3.095 | 3.141(5) | 3.114(7) |
| M2-X2 | 2.54(2) | 2.623(7) | 2.50(3) | 2.57(2) | 2.610(10) | 2.699(7) |
| M2-X2 | 2.72(2) | 2.622(8) | 2.67(3 ) | 2.646(19) | 2.657(11) | 2.759(7) |
| M2-X3 (x2) | 2.591(12) | 2.617(7) | 2.572(15) | 2.609(11) | 2.630(7) | 2.755(7) |
| M2-X3 (x2) | 2.488(14) | 2.507(6) | 2.544(17) | 2.503(12) | 2.533(7) | 2.686(7) |
| Average | 2.687 | 2.702 | 2.685(14) | 2.693 | 2.718 | 2.824 |
| Si-X1 | 1.623(16) | 1.612(9) | 1.62(2) | 1.578(19) | 1.622(11) | 1.614(7) |
| Si-X2 | 1.60(2) | 1.635(8) | 1.63(3) | 1.60(2) | 1.682 (18) | 1.652(7) |
| Si-X3 (x2) | 1.632(15) | 1.616(6) | 1.585(19) | 1.615(13) | 1.677(10) | 1.632(7) |
| a (Å) | 5.6436(14) | 5.682(1) | 5.63246 | 5.665(2) | 5.733(4) | 5.805(1) |
| b(Å) | 7.10719(17) | 7.090(1) | 7.11675 | 7.137(3) | 7.316(5) | 7.499(1) |
| c(Å) | 9.8062(2) | 9.773(2) | 9.7998 | 9.767(3) | 9.902(7) | 10.200(3) |
| V ($Å^3$) | 393.329(16) | 393.7 | 392.825 | 396 | 415.3(5) | 444.02 |

(a) From powder X-ray diffraction data for $LaSrSiO_3N$ and $LaEuSiO_3N$, powder neutron diffraction data for $LaBaSiO_3N$ and single crystal X-ray diffraction for $Sr_2SiO_4$ (Catti, M.; Gazzoni, G.; Ivaldi, G.; Zanini, G. *Acta Cryst.* **1983**, *B39*, 674-679), $Eu_2SiO_4$ ( Marchand, R.; l'Harildoon, P.; Laurent, Y. *J. Solid State Chem.* , **1978**, 24, 71-76) and $Ba_2SiO_4$ (Grosse, H-P; Tillmanns, E. *Cryst. Struct. Comm.* **1974**, *3*, 599-602.).

**Table S5. Bond Valence Sums (BVS) for $LaMSiO_3N$ compounds**

| Site | $LaSrSiO_3N$ | $LaBaSiO_3N$ | $LaEuSiO_3N$ |
|---|---|---|---|
| La1/ M1 | 2.05(3)/1.69(2) | 1.71(1)/2.35(2)[a] | 2.02(4)/1.88(3) |
| La2/ M2 | 2.98(5)/2.44(3) | 2.74(2)/3.78(3)[a] | 2.96(5)/1.97(7) |
| Si | 4.36(8) | 3.86(5) | 4.5(1) |
| O1 | 1.98(5) | 2.04(3) | 1.97(7) |
| O2/N2 | 2.13(7)/2.96(9) | 2.03(4)/3.02(6) | 2.10(9)/3.1(1) |
| O3/N3 | 2.03(4)/2.85(6) | 1.99(3)/2.95(4) | 2.14(6)/3.15(8) |

(a) Deviations of BVS with respect to the formal charges of the cations for these sites are larger because of the mixed occupation and the differences between the ionic radii of $Ba^{2+}$ and $La^{3+}$.

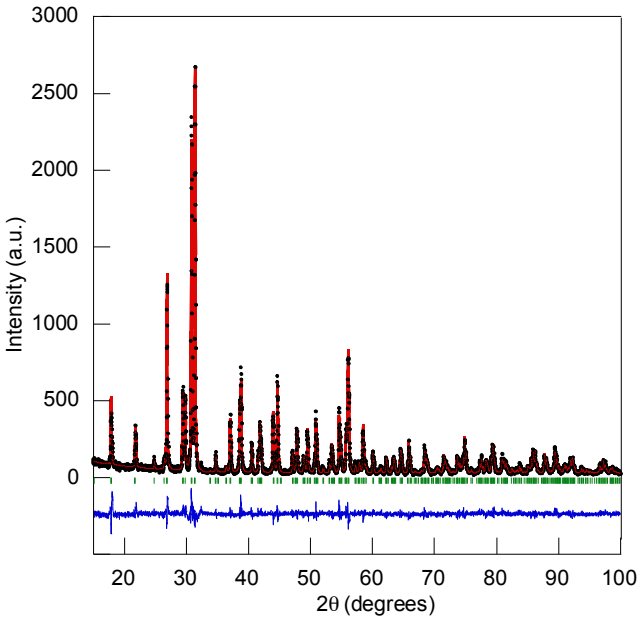


Figure S1. Observed and calculated powder X-ray diffraction patterns for $LaSrSiO_3N$.

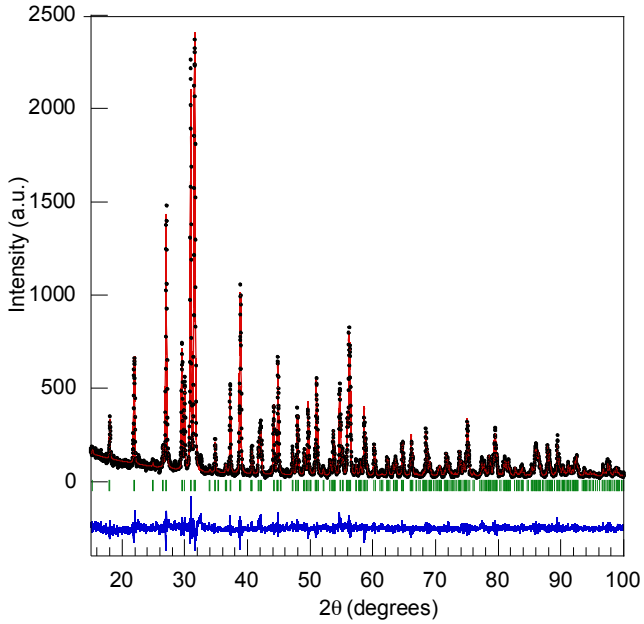


Figure S2. Observed and calculated powder X-ray diffraction patterns for $LaEuSiO_3N$.

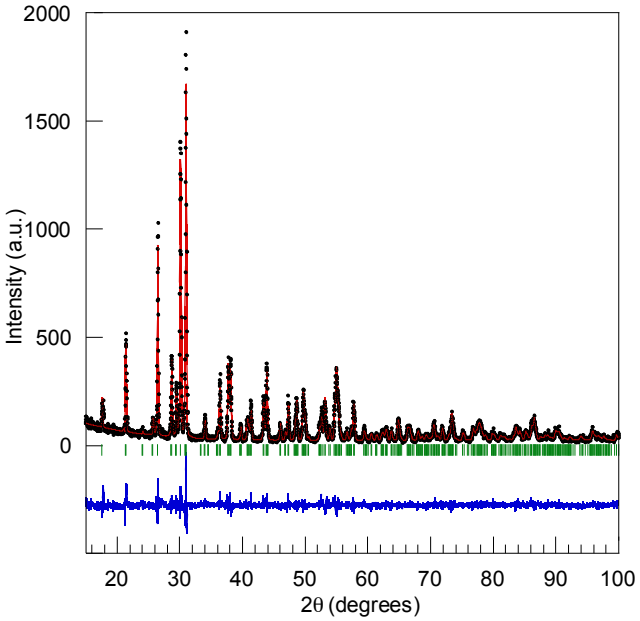


Figure S3. Observed and calculated powder X-ray diffraction patterns for $LaBaSiO_3N$.

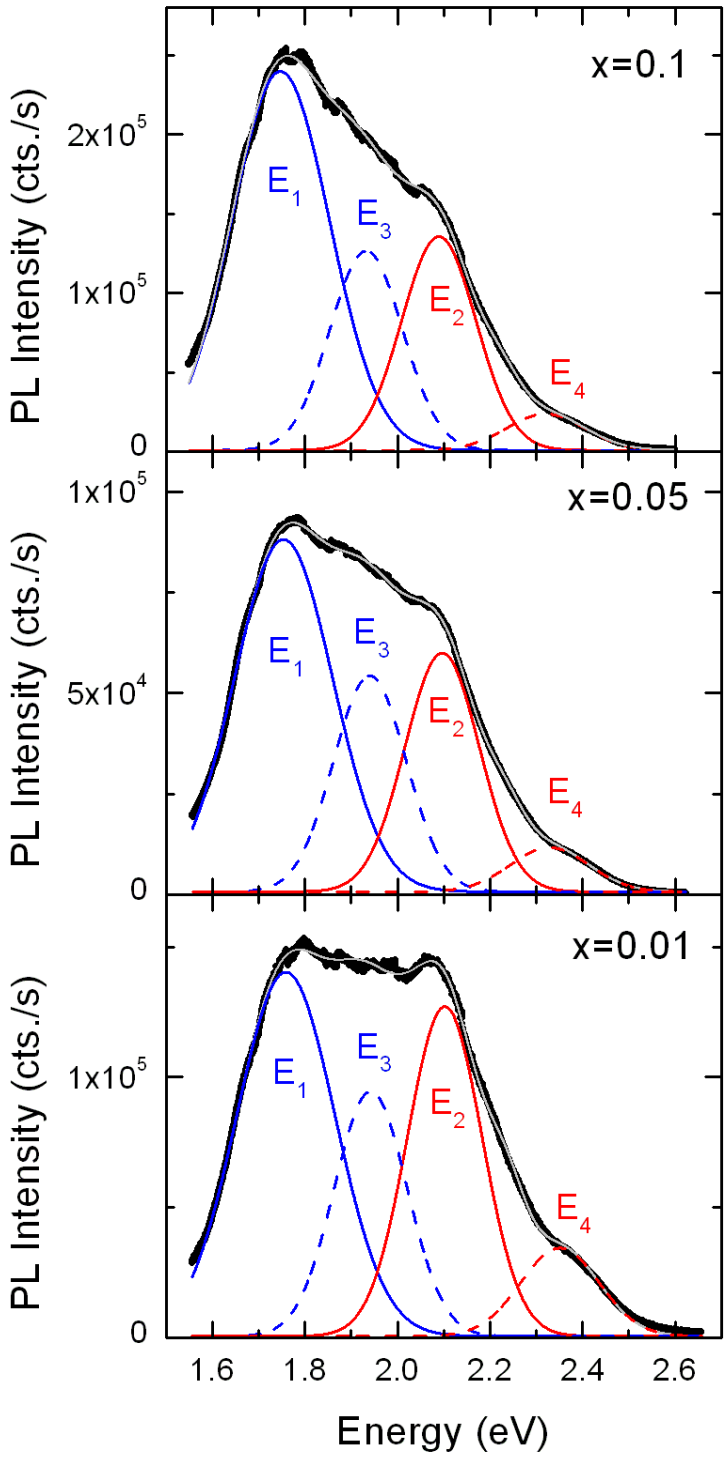


Figure S4. Deconvolution of emission spectra of $LaSr_{1-x}Eu_xSiO_3N$ under excitation at 405 nm. Bands corresponding to M1 and M2 sites are depicted with red and blue lines respectively.

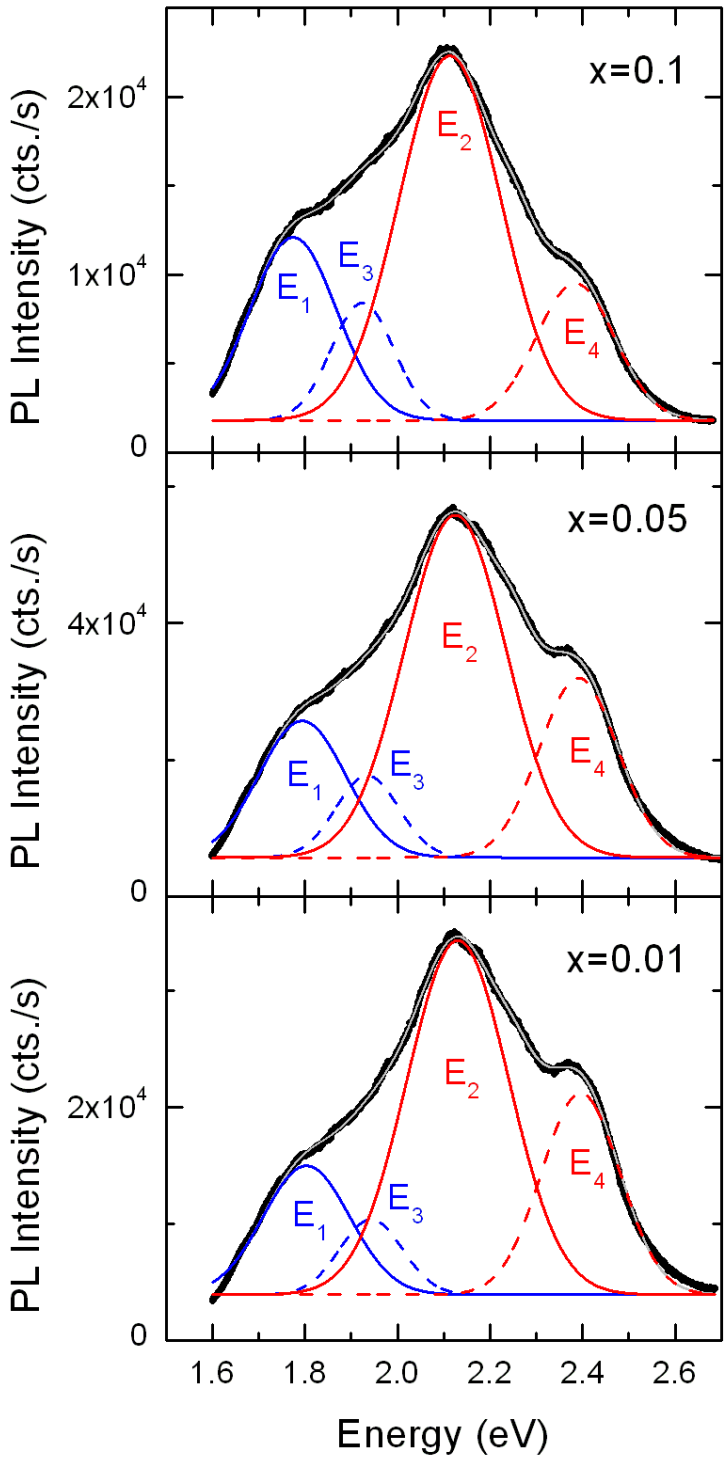


Figure S5. Deconvolution of emission spectra of $La_{1-x}Ce_xSrSiO_3N$ under excitation at 405 nm. Bands corresponding to M1 and M2 sites are depicted with red and blue lines respectively.

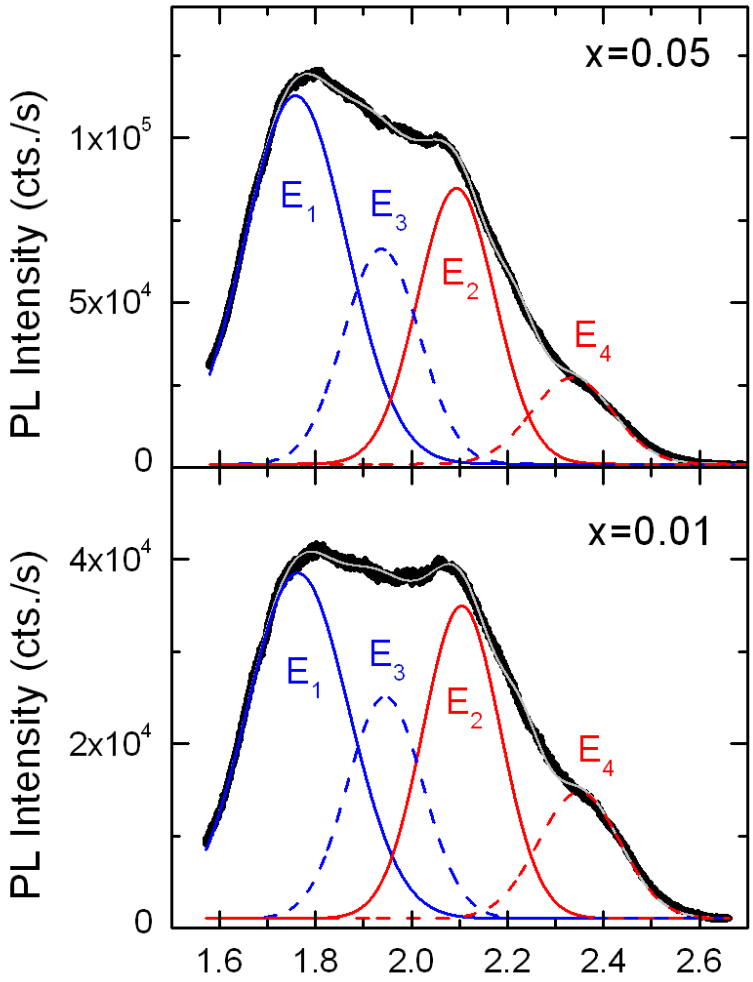


Figure S6. Deconvolution of emission spectra of $LaBa_{1-x}Eu_xSiO_3N$ under excitation at 405 nm. Bands corresponding to M1 and M2 sites are depicted with red and blue lines respectively.